HHS Public Access

Author manuscript

Eur Radiol. Author manuscript; available in PMC 2022 December 01.

Published in final edited form as:

Eur Radiol. 2021 December ; 31(12): 9428–9435. doi:10.1007/s00330-021-08071-w.

Opportunistic application of phantom-less calibration methods for fracture risk prediction using QCT/FEA

Maria Prado[1], **Sundeep Khosla**[2], **Christopher Chaput**[3], **Hugo Giambini**[1]

[1]Department of Biomedical Engineering and Chemical Engineering, University of Texas at San Antonio, San Antonio, TX, USA.

[2]Kogod Center on Aging and Division of Endocrinology, Mayo Clinic College of Medicine, Mayo Clinic, Rochester, MN, USA.

[3]Department of Orthopedics, The University of Texas Health Science Center at San Antonio, San Antonio, TX, USA

Abstract

Objectives: Quantitative computed-tomography (QCT)-based finite element analysis (FEA) implements a calibration phantom to estimate bone mineral density (BMD) and assign material properties to the models. The objectives of this study were to 1) propose robust phantom-less calibration methods, using subject-specific tissues, to obtain vertebral fracture properties estimations using QCT/FEA; and 2) correlate QCT/FEA predictions to DXA values of areal BMD.

Methods: Eighty of a cohort of 111 clinical QCT scans were used to obtain subject-specific parameters using a phantom calibration approach and for the development of the phantom-less calibration equations. Equations were developed based on the HU measured from various soft tissues and regions, and using multiple linear regression analyses. 31 additional QCT scans were used for cross-validation of QCT/FEA estimated fracture loads from the L_3 vertebrae based on the phantom and phantom-less equations. Finally, QCT/FEA-predicted fracture loads were correlated with aBMD obtained from DXA

Results: Overall, 217 QCT/FEA models from 31 subjects (20 females, 11 men) with mean ages of 69.6 (13.1) and 67.3 (14) were used to cross-validate the phantom-less equations and assess bone strength. The proposed phantom-less equations showed high correlations with phantom-based estimates of BMD (99%). Cross-validation of QCT/FEA-predicted fracture loads from phantom-less equations and phantom-specific outcomes resulted in high correlations for all proposed methods (0.94 – 0.99). QCT/FEA correlation outcomes from the phantom-less equations and DXA-aBMD were moderately high (0.64 – 0.68).

Conclusions: The proposed QCT/FEA subject-specific phantom-less calibration methods demonstrated the potential to be applied to both prospective and retrospective applications in the clinical setting.

Corresponding Author: Hugo Giambini, Ph.D., One UTSA Circle, San Antonio, TX 78249, The University of Texas at San Antonio, Phone: 210-458-8182, hugo.giambini@utsa.edu.

Keywords

Bone Density; Bone Fractures; Finite Element Analysis; Quantitative computed-tomography; Phantom-less; Spine

Introduction

Osteoporosis is a public health concern associated with an increase in fracture risk. In this setting, vertebrae are the second most common affected bones with a fracture incidence exceeding 1.4 million annual cases in the U.S. [1–4]. Dual-energy x-ray absorptiometry (DXA) is the most common method for estimation of bone mineral density (BMD) and fracture risk in the clinical setting [5, 6]. However, DXA presents several limitations such as not being able to assess the three-dimensional (3D) details of the vertebrae and potential overestimation of BMD values. This latter limitation is mostly observed in patients presenting with degeneration in the spine and in overweight patients, possibly leading to under-treatment of clinically significant bone loss and an increase in fracture risk [4, 7–9]. Thus, there is a critical need to improve fracture risk detection and treatment.

Measurements of Hounsfield units (HU) from the CT images have been previously used to evaluate longitudinal bone loss [10], osteoporosis diagnosis and prevalent fractures [11, 12], and fracture properties of vertebrae [13]. However, this approach presents inherent limitations. First, while *in-vivo* HU attenuation of vertebral trabecular bone can be correlated with prevalent vertebral compression fractures observed at other regions of the spine, and with DXA-defined osteoporosis thresholds [11, 12], it is important to acknowledge that the process does not predict fracture properties and the load bearing capacity of the vertebrae at the measured location. Although HU values from a single-slice measurement correlates with experimentally-measured fracture force outcomes [13], this correlation is not strong, possibly due to trabecular bone microarchitecture and density varying from the superior to the inferior regions of the vertebrae. On the other hand, quantitative computed tomography (QCT) combined with finite element analysis (FEA) has become a reliable tool to asses fracture risk. QCT/FEA has been shown to significantly improve the prediction of fracture properties and the risk for fracture as it considers 3D bone geometry, bone distribution, and allows for material properties estimates from the QCT images [4, 6, 9, 14–17].

BMD distribution in the target bone as well as its conversion to Young's modulus using empirical material equations are critical steps in the development of subject-specific QCT/FEA models. To obtain subject-specific BMD measurements, a calibration phantom – employed for the conversion of HU from the CT images to BMD – is placed underneath the subject during the scanning process. However, these calibration phantoms are expensive, are not always available, and increase the logistic burden during imaging, such as the addition of separate mattresses for the patients to lie on and logistical challenges for research studies involving more than one clinical setting [8, 18]. Pre-calibration of the CT-scanner with a calibration phantom has been introduced as an alternative approach to overcome the use of a phantom in each scan. Although this is a better option than having no calibration

in the process, this method is not specific to each subject, does not consider important individual variations such as body size, and cannot be applied retrospectively [2]. An additional approach is the use of a patient-specific phantom-less calibration technique. This process uses the patient's own tissues, such as fat and muscle, as the calibrating reference materials to convert HU to BMD [2, 7, 9, 16]. With this approach, the reference regions of interest (ROIs) are located close to the vertebral bodies, avoiding any beam hardening and scattering effects, and reducing factors associated to subject body size and the relative positions between patient and calibration phantom [5, 16, 18, 19]. The ROIs are then implemented to obtain a relationship between HU and BMD, yielding high reliability and accuracy of outcomes [2, 5, 6, 8, 18]. Although phantom-less calibration is a promising method for replacing the use of a phantom during QCT scans and performing prospective analyses, to our knowledge, there are no studies describing the relationship between these subject-specific tissues and BMD, and QCT/FEA vertebral fracture prediction outcomes [6, 8, 20]. The phantom-less calibration approach can be used to develop QCT/FEA subject-specific models for fracture risk assessment and surgical planning on routine CT scans acquired for other clinical purposes, without additional radiation exposure and substantial costs.

The aim of this study was to propose robust phantom-less calibration methods, using subject-specific tissues, which could be applied prospectively and retrospectively to databases of CT scans to obtain fracture properties estimations using QCT/FEA. In this study, we developed phantom-less calibration equations using a population cohort and evaluated these equations using QCT/FEA to obtain vertebral fracture loads. Then, the fracture loads obtained with QCT/FEA from the various phantom-less equations were correlated to those obtained using a calibration phantom and to BMD values obtained using DXA.

Methods

Study population and CT scans

The study population comprised the use of pre-existing DXA and QCT scans that had been collected as part of ongoing studies from the Mayo Clinic [21]. All subjects provided written informed consent and the study was approved by the Mayo Clinic Institutional Review Board. DXA imaging of subjects was performed using a single Lunar Prodigy (GE Healthcare) scanner following a standardized clinical scanning and analysis protocol to obtain areal BMD (aBMD) of the spine. Spine QCT scans were performed using a Siemens Sensation-64 CT scanner (Siemens Healthcare). QCT images were obtained using a standardized protocol with the following settings: 120 kVp, 67 mA, 0.8 s rotation time, 0.75 pitch, 20 s scan time, 2.0 mm image thickness, 7.5 mm/rotation table speed, and 10 mm collimation; and reconstructed using a soft kernel (B30). The subjects were scanned together with a calibration phantom (Mindways Inc.) included in the scan field-of-view. The calibration phantom contained five rods of known reference material (K_2HPO_4) used for conversion of HU to K_2HPO_4 equivalent density, as a surrogate for BMD. The QCT scans included a total of 111 subjects (70 females and 41 males). Eighty (50 women and 30 men) of the 111 scans were used to obtain subject-specific parameters using a phantom calibration

approach and for the development of phantom-less calibration equations. The remaining 31 scans, including subjects with t-scores in the osteoporotic, osteopenic, and normal ranges, were used for cross-validation of fracture loads using QCT/FEA based on the phantom calibration and phantom-less approach. Subject demographics were also collected as part of the study and are shown in Table 1.

Phantom-specific calibration

Eighty (80) QCT scans were used to obtain subject-specific parameters using a phantom calibration approach. QCT images were imported into Mimics software (Materialise), the L_3 vertebra identified, and a region-of-interest (ROI) placed within the center of the vertebra at a mid-slice to obtain a mean HU value for trabecular bone. Following the phantom manufacturer specifications, HU was then converted into BMD as follows [13]:

$$\rho_{ash} = K_2HPO_4 = BMD_{(unknow)} = \frac{\mu_{ROI} - \beta_{CT}}{\sigma_{CT}},$$

where β_{CT} relates an imaging technique-specific parameter characteristic of the CT number scale, and σ_{CT} characterizes the response of the CT scanner to changes in pure K_2HPO_4. Outcomes from this process included individual subject-specific β_{CT} and σ_{CT} values, and an average of these values representing the population cohort.

Phantom-less calibration

The same 80 subjects used for subject-specific phantom calibration were used to obtain phantom-less calibration equations. A series of phantom-less calibration equations were developed based on the HU measured from various tissues and regions: air (A), fat (F), psoas muscle (M), and subject perimeter (P). In the same middle slice used during the phantom calibration process, ROIs (20–30 mm^2) were placed in the (A), (F), (M), and (P) to obtain average HU values, respectively (Fig. 1). These HU values, together with the HU value from the L_3 vertebra of interest, were implemented in a multiple linear regression analyses to obtain phantom-less equations that would estimate the BMD value of the L_3 ROI obtained using subject-specific phantom equations. The HU values obtained for the ROIs [(A), (F), (M), (P), and (L_3)], were used to develop various phantom-less calibration functions:

$$BMD_{Phantom-less} = C_1 + C_2 \times (\boldsymbol{P}) + C_3 \times (\boldsymbol{A}) + C_4 \times (\boldsymbol{F}) + C_5 \times (\boldsymbol{M}) + C_6 \times (\boldsymbol{HU})$$

where coefficients (C_1 to C_6) were obtained using multiple regression analyses detailed in the statistical section.

QCT/FEA fracture prediction

Thirty-one (31; 20 females and 11 males) subjects were used to cross-validate the phantom-less equations and the average phantom-specific β_{CT} and σ_{CT}, with phantom-specific fracture load outcomes. The QCT/FEA process has been previously validated and described in detail [22]. Briefly, models of the L_3 vertebrae were created from the CT-DICOM

images by manual segmentation of the vertebral bodies using Mimics. The cortical and trabecular bones were manually segmented to obtain a 3D geometry and a top and bottom layer were included to allow for uniform boundary conditions and load application. Voxel volume meshes were created maintaining a ratio of 1:1 (FE-voxel:CT-voxel), and each voxel was assigned an HU value corresponding to the CT voxel in the image. To obtain subject-specific properties, the σ_{CT} and β_{CT} obtained from the individual phantom calibration process were used to convert the HUs from each voxel to equivalent K_2HPO_4 density. Similarly, for a non-subject-specific approach, the average phantom-specific σ_{CT} and β_{CT} values – obtained from the 80-patient cohort – were used to convert HUs to equivalent K_2HPO_4 density. Additionally, five phantom-less equations were implemented to convert HU in the L_3 vertebrae to K_2HPO_4. Thus, QCT/FEA fracture loads were estimated using three different approaches: **1)** subject-specific calibration phantom; **2)** non-subject-specific phantom calibration parameters; and **3)** five different phantom-less calibration equations.

QCT/FEA models of the L_3 vertebra were imported into ANSYS Mechanical APDL (ANSYS) where a Young's modulus value (E, [MPa]) was assigned to each finite element using a power-law ash density-modulus relation ($E = 4730 \times \rho_{app}^{1.56}$) [23], where a ratio between ash and apparent density $\left(\rho_{ash}/\rho_{app}\right)$ of 0.6 was used to obtain ash density. Top and bottom layers were assigned an E = 2500 MPa; the bottom layer was fixed in all directions while a displacement was applied to the top layer to induce compression. Fracture load was estimated as a function of vertebral stiffness (K_{FE}) and height (H) of the vertebra [24] as follows:

$$F_{FE} = 0.0068 K_{FE} H$$

Our previous studies show the QCT/FEA approach can predict up-to 89% of the experimental fracture loads (supplemental material, [22]). All aspects of the FE modeling were kept the same during the study while only changing the material assignment approach based on the various phantom-based and phantom-less equations.

Statistical analyses

JMP Pro-14 (SAS Institute Inc.) was used for all statistical analyses. Coefficient of determination (R^2), calculated with respect to the goodness of fit (Y = mX + b), were obtained using all 111 subjects to evaluate the effect of age on QCT-estimated BMD outcomes obtained using the subject-specific phantom calibration equation. From the cohort of 80-patients, the HU values from the (A), (F), (M), (P), and (L_3), were used to develop phantom-less calibration equations using a multiple linear regression model and the subject-specific L_3-BMD estimated values. Briefly, the ROI from the L_3 was converted from HU to BMD using the calibration phantom. Then, this BMD dependent variable was predicted based on the independent variables (A, F, M, P, and the HU at the L_3). Using the measured HU values, regression equations were obtained by combining PAFM, PFM, AFM, FM, and M. Statistical significance and R^2 were obtained for each equation with respect to the subject-specific calibration phantom outcomes.

Coefficients of determination ($\hat{R}^2$) with respect to Y = X were obtained for the QCT/FEA predicted fracture loads based on the 5 phantom-less equations and the 1 non-subject-specific equation, with respect to the subject-specific phantom calibration equation outcomes. Additionally, QCT/FEA predicted fracture loads from the 31 subjects and from all 7 equations (5 phantom-less equations + 1 non-subject-specific equation + 1 subject-specific equation) were correlated with aBMD obtained from DXA. The level of significance was set at $p<0.05$.

Results

A cohort of 111 patients was used to develop phantom-less calibration methods to allow for prediction of vertebral fracture properties using QCT/FEA. Figure 2 shows QCT-estimated BMD using the calibration phantom from the 111 subjects vs. age and sex. Correlation coefficients ($\hat{R}^2$) for BMD outcomes between the phantom calibration method and the proposed phantom-less methods are shown in Table 2. All phantom-less equations showed high correlations with the phantom-based BMD outcomes. A total of 217 QCT/FEA models were run [31 subjects x (5 phantom-less equations + 1 non-subject-specific equation + 1 subject-specific equation)] to estimate vertebral fracture loads. Fracture loads predicted from the QCT/FEA models developed with the calibration phantom vs. those developed using the phantom-less equations and the non-subject-specific phantom calibration (average σ_{CT} and β_{CT}) were assessed in terms of model accuracy (Table 3). Correlation outcomes ($\hat{R}^2$) for the non-subject-specific equation and the phantom-less calibration equations were high, ranging between 0.94–0.99. The highest accuracy was obtained for the non-subject-specific equation, and PAFM, PFM and AFM phantom-less equations, with $\hat{R}^2$ values of 0.99 (Table 3).

Coefficients of determination (R^2) between aBMD values obtained from DXA and the predicted fracture loads from QCT/FEA using the **1)** calibration phantom, the **2)** phantom-less equations, and the **3)** non-subject-specific equation are shown in Table 4. Correlation outcomes for all cases were moderately high, ranging from 0.64–0.68. Similar correlation outcomes were obtained for three of the phantom-less equations and the non-subject-specific equation when compared to the calibration phantom process. The FM and M phantom-less equations showed lower correlations, 0.64 and 0.67, respectively.

Discussion

This study aimed to develop calibration methods, allowing for the conversion of HU to BMD values using a phantom-less calibration approach, to obtain vertebral fracture properties using QCT/FEA. Outcomes demonstrated that the proposed phantom-less methods can successfully be used in QCT/FEA to estimate vertebral failure loads that are highly accurate and correlate with fracture loads obtained using the traditional phantom calibration method.

A strong correlation between the phantom calibration, gold standard for quantitative CT and QCT/FEA, and the proposed phantom-less equations were obtained when comparing BMD

values and estimated fracture load outcomes. Equations using solely fat and muscle highly correlated with outcomes using the calibration phantom ($\widehat{R}^2$ of 0.98 and 0.94, respectively). On the other hand, these correlations could be significantly improved by incorporating the perimeter of the patient ($\widehat{R}^2$=0.99). Additionally, a second calibration method using a non-subject-specific approach resulted in an accuracy ($\widehat{R}^2$) of 0.99 when compared to the predicted values using the phantom. In order to validate and evaluate the precision of the predicted fracture load outcomes, aBMD values were correlated to QCT/FEA predictions showing moderate correlations (68%).

While other studies have proposed phantom-less calibration methods, these presents several limitations and significant shortcomings [6, 8, 16, 18, 20]. For example, none of the previous studies have evaluated the differences between the combinations presented in this study; some relate to femur and not vertebrae; a small number of patients/subjects was evaluated; and more importantly, the phantom-less equations may not be described. Lee et al. developed a phantom-less approach using a cohort of 40 subjects and performed QCT/FEA of vertebrae, concluding that their internal calibration process was as good as the phantom calibration [16]. Similarly, Eggermont et al. developed an internal calibration process to convert HU-to-BMD and evaluated femur fracture properties using QCT/FEA in 57 advanced cancer patients [8]. Results showed high correlations (~0.94) between their phantom-less method and the phantom calibration. While these previous studies show the feasibility of the approach, unfortunately, both studies do not present their internal calibration equations, and Eggermont et al. investigates patients with cancer metastasis to the femur, which, while possibly presenting a similar HU values compared to a normal bone, could differ in their intrinsic bone material properties. On the other hand, Han Lee et al. developed a phantom-less calibration method using 39 subjects and performed QCT/FEA of the L2 vertebrae [6]. The group found a high correlation between the estimated BMD using the phantom calibration and the phantom-less approach (0.99). However, the phantom-less approach only included measurements of the subject's perimeter; the QCT/FEA process did not estimate failure; the predicted outcomes were not correlated to DXA values; and more importantly, the phantom-less equation was not cross-validated against other cohorts.

It is well known that patients' physical factors such as perimeter can influence the accuracy of the phantom-less calibration method as this can affect the attenuation of radiation and therefore the HU values [6]. By including the waist circumference, a routine abdomen-pelvic, or pelvic CT obtained without a reference phantom has the potential to be used for a phantom-less calibration process using the methodologies proposed in this study. Additionally, the use of internal reference tissues, particularly fat and muscle, offer reliability because of their proximity to the vertebral body reflecting more accurately the local changes in the x-ray spectra and scatter distribution at the target tissue [19]. In clinical practice, phantom-less calibration methods can be critical for identifying patients that are at high risk for fracture. With the proposed phantom-less calibration methods, HU-to-BMD conversion and failure load evaluations of the spine could be extended to retrospective analysis of existing CT images or prospectively avoiding the logistic limitations of the phantom calibration [9, 20]. QCT/FEA analysis without the use of traditional calibration phantoms would allow region-specific evaluation of bone density and quality in the spine,

taking advantage of the significant amount of bone information and health within the CT image [7]. In addition, the proposed methods could replace the use of DXA in the future, when CT-scans of subjects are available, avoiding additional radiation exposure as well as a reduction in healthcare costs. Furthermore, the techniques described in this study could be utilized by orthopedic and spinal surgeons to address patients with poor bone quality preemptively with treatment of osteoporosis or with the use of additional instrumentation to improve fixation and prevent catastrophic hardware failure.

A pre-calibration method has been recently introduced to allow for the quantification of BMD without the use of calibration phantom. However, this process does not consider the patients' physical factors that affect HU values, showing poor repeatability [6]. Placing a phantom underneath the patient also has its inherent limitations. Patient body size, shape and position in the scan field will affect CT numbers and can introduce a shift of these values over the scan field [19]. Having a phantom in a peripheral location underneath the subject magnifies these problems and can lead to inaccurate BMD estimations [5, 19, 25]. Thus, a phantom-less approach would overcome many of the current limitation in this process, such as the use of tissues adjacent to the target bone, accounting for potential beam-hardening and scattering artifacts present in the scan [5, 19].

This study is not without limitations. First, the phantom-less calibration equations were developed using a single scanner with a clinical CT scanning protocol. While using only a single scanner, the process resulted in robust equations that were cross-validated with a large secondary cohort of patients. Second, the proposed methodology is only considered for the spine, and other bone sites such as the femur were not evaluated. Additionally, while the QCT/FEA process has been previously validated using cadaveric studies, the outcomes from the phantom-less QCT/FEA approach, obtained using data from live subjects, cannot be validated for fracture properties. However, predictions were shown to be moderately correlated to aBMD outcomes from DXA. Future studies should consider proposing equations using various scanners and other bone sites.

Conclusion

The use of phantom-less calibration methods for conversion of HU-to-BMD from CT images using the patients' reference tissues and regions emerges as an accurate method over phantom-based calibration estimations. QCT/FEA predictions of vertebral fracture loads using the phantom-less approach highly correlated to values obtained using the calibration phantom. The QCT/FEA phantom-less approach presented in this study can be used for osteoporosis diagnosis and fracture risk estimations from images previously acquired for other purposes, or prospectively without the use of a calibration phantom, minimizing logistic controls and reproducibility errors associated with external reference phantoms.

Supplementary Material

Refer to Web version on PubMed Central for supplementary material.

Abbreviations:

QCT	Quantitative computed tomography
FEA	Finite element analysis
DXA	Dual x-ray absorptiometry
BMD	Bone mineral density
HU	Hounsfield unit
ROI	region of interest
K_2HPO_4	Potassium phosphate
DICOM	Digital Imaging and Communications in Medicine

References

1. Johannesdottir F, Allaire B, and Bouxsein ML, Fracture Prediction by Computed Tomography and Finite Element Analysis: Current and Future Perspectives. Curr Osteoporos Rep, 2018. 16(4): p. 411–422. doi: 10.1007/s11914-018-0450-z.. [PubMed: 29846870]
2. Kaesmacher J, Liebl H, Baum T, and Kirschke JS, Bone Mineral Density Estimations From Routine Multidetector Computed Tomography: A Comparative Study of Contrast and Calibration Effects. J Comput Assist Tomogr, 2017. 41(2): p. 217–223. doi: 10.1097/RCT.0000000000000518.. [PubMed: 27798444]
3. Schreiber JJ, Anderson PA, and Hsu WK, Use of computed tomography for assessing bone mineral density. Neurosurg Focus, 2014. 37(1): p. E4. doi: 10.3171/2014.5.FOCUS1483..
4. Valentinitsch A, Trebeschi S, Kaesmacher J, et al. , Opportunistic osteoporosis screening in multi-detector CT images via local classification of textures. Osteoporos Int, 2019. 30(6): p. 1275–1285. doi: 10.1007/s00198-019-04910-1.. [PubMed: 30830261]
5. Engelke K, Lang T, Khosla S, et al. , Clinical Use of Quantitative Computed Tomography-Based Advanced Techniques in the Management of Osteoporosis in Adults: the 2015 ISCD Official Positions-Part III. J Clin Densitom, 2015. 18(3): p. 393–407. doi: 10.1016/j.jocd.2015.06.010.. [PubMed: 26277853]
6. Lee YH, Kim JJ, and Jang IG, Patient-Specific Phantomless Estimation of Bone Mineral Density and Its Effects on Finite Element Analysis Results: A Feasibility Study. Comput Math Methods Med, 2019. 2019: p. 4102410. doi: 10.1155/2019/4102410..
7. Brett AD and Brown JK, Quantitative computed tomography and opportunistic bone density screening by dual use of computed tomography scans. J Orthop Translat, 2015. 3(4): p. 178–184. doi: 10.1016/j.jot.2015.08.006.. [PubMed: 30035056]
8. Eggermont F, Verdonschot N, van der Linden Y, and Tanck E, Calibration with or without phantom for fracture risk prediction in cancer patients with femoral bone metastases using CT-based finite element models. PLoS One, 2019. 14(7): p. e0220564. doi: 10.1371/journal.pone.0220564.. [PubMed: 31361790]
9. Keaveny TM, Clarke BL, Cosman F, et al. , Biomechanical Computed Tomography analysis (BCT) for clinical assessment of osteoporosis. Osteoporos Int, 2020. 31(6): p. 1025–1048. doi: 10.1007/s00198-020-05384-2.. [PubMed: 32335687]
10. Giambini H, Khosla S, Nassr A, Zhao C, and An KN, Longitudinal changes in lumbar bone mineral density distribution may increase the risk of wedge fractures. Clin Biomech (Bristol, Avon), 2013. 28(1): p. 10–4. doi: 10.1016/j.clinbiomech.2012.10.005..
11. Graffy PM, Lee SJ, Ziemlewicz TJ, and Pickhardt PJ, Prevalence of Vertebral Compression Fractures on Routine CT Scans According to L1 Trabecular Attenuation: Determining Relevant

Thresholds for Opportunistic Osteoporosis Screening. AJR Am J Roentgenol, 2017. 209(3): p. 491–496. doi: 10.2214/AJR.17.17853.. [PubMed: 28639828]

12. Pickhardt PJ, Pooler BD, Lauder T, et al. , Opportunistic screening for osteoporosis using abdominal computed tomography scans obtained for other indications. Ann Intern Med, 2013. 158(8): p. 588–95. doi: 10.7326/0003-4819-158-8-201304160-00003.. [PubMed: 23588747]
13. Catano Jimenez S, Saldarriaga S, Chaput CD, and Giambini H, Dual-energy estimates of volumetric bone mineral densities in the lumbar spine using quantitative computed tomography better correlate with fracture properties when compared to single-energy BMD outcomes. Bone, 2020. 130: p. 115100. doi: 10.1016/j.bone.2019.115100.. [PubMed: 31678491]
14. Bevill G, Eswaran SK, Farahmand F, and Keaveny TM, The influence of boundary conditions and loading mode on high-resolution finite element-computed trabecular tissue properties. Bone, 2009. 44(4): p. 573–8. doi: 10.1016/j.bone.2008.11.015.. [PubMed: 19110082]
15. Giambini H, Qin X, Dragomir-Daescu D, An KN, and Nassr A, Specimen-specific vertebral fracture modeling: a feasibility study using the extended finite element method. Med Biol Eng Comput, 2016. 54(4): p. 583–93. doi: 10.1007/s11517-015-1348-x.. [PubMed: 26239163]
16. Lee DC, Hoffmann PF, Kopperdahl DL, and Keaveny TM, Phantomless calibration of CT scans for measurement of BMD and bone strength-Inter-operator reanalysis precision. Bone, 2017. 103: p. 325–333. doi: 10.1016/j.bone.2017.07.029.. [PubMed: 28778598]
17. Mao SS, Li D, Luo Y, Syed YS, and Budoff MJ, Application of quantitative computed tomography for assessment of trabecular bone mineral density, microarchitecture and mechanical property. Clin Imaging, 2016. 40(2): p. 330–8. doi: 10.1016/j.clinimag.2015.09.016.. [PubMed: 26602163]
18. Mueller DK, Kutscherenko A, Bartel H, et al. , Phantom-less QCT BMD system as screening tool for osteoporosis without additional radiation. Eur J Radiol, 2011. 79(3): p. 375–81. doi: 10.1016/j.ejrad.2010.02.008.. [PubMed: 20223609]
19. Boden SD, Goodenough DJ, Stockham CD, et al. , Precise measurement of vertebral bone density using computed tomography without the use of an external reference phantom. J Digit Imaging, 1989. 2(1): p. 31–8. doi: 10.1007/BF03168013. [PubMed: 2488150]
20. Weaver AA, Beavers KM, Hightower RC, et al. , Lumbar Bone Mineral Density Phantomless Computed Tomography Measurements and Correlation with Age and Fracture Incidence. Traffic Inj Prev, 2015. 16 Suppl 2: p. S153–60. doi: 10.1080/15389588.2015.1054029..
21. Riggs BL, Melton Iii LJ 3rd, Robb RA, et al. , Population-based study of age and sex differences in bone volumetric density, size, geometry, and structure at different skeletal sites. J Bone Miner Res, 2004. 19(12): p. 1945–54. doi: 10.1359/JBMR.040916.. [PubMed: 15537436]
22. Prado M, Rezaei A, and Giambini H, Density-Dependent Material and Failure Criteria Equations Highly Affect the Accuracy and Precision of QCT/FEA-Based Predictions of Osteoporotic Vertebral Fracture Properties. Ann Biomed Eng, 2020. doi: 10.1007/s10439-020-02595-w..
23. Morgan EF, Bayraktar HH, and Keaveny TM, Trabecular bone modulus-density relationships depend on anatomic site. J Biomech, 2003. 36(7): p. 897–904.. [PubMed: 12757797]
24. Crawford RP, Cann CE, and Keaveny TM, Finite element models predict in vitro vertebral body compressive strength better than quantitative computed tomography. Bone, 2003. 33(4): p. 744–750. doi: 10.1016/s8756-3282(03)00210-2. [PubMed: 14555280]
25. Benca E, Amini M, and Pahr DH, Effect of CT imaging on the accuracy of the finite element modelling in bone. Eur Radiol Exp, 2020. 4(1): p. 51. doi: 10.1186/s41747-020-00180-3. [PubMed: 32869123]

Key-Points:

- QCT/FEA overcomes the disadvantages of DXA and improves fracture properties predictions of vertebrae.
- QCT/FEA fracture estimates using the phantom-less approach highly correlated to values obtained using a calibration phantom.
- Phantom-less estimations of BMD is a promising method that can be used prospectively and retrospectively in the clinical setting.
- QCT/FEA predictions using a phantom-less approach is an accurate alternative over phantom-based methods.

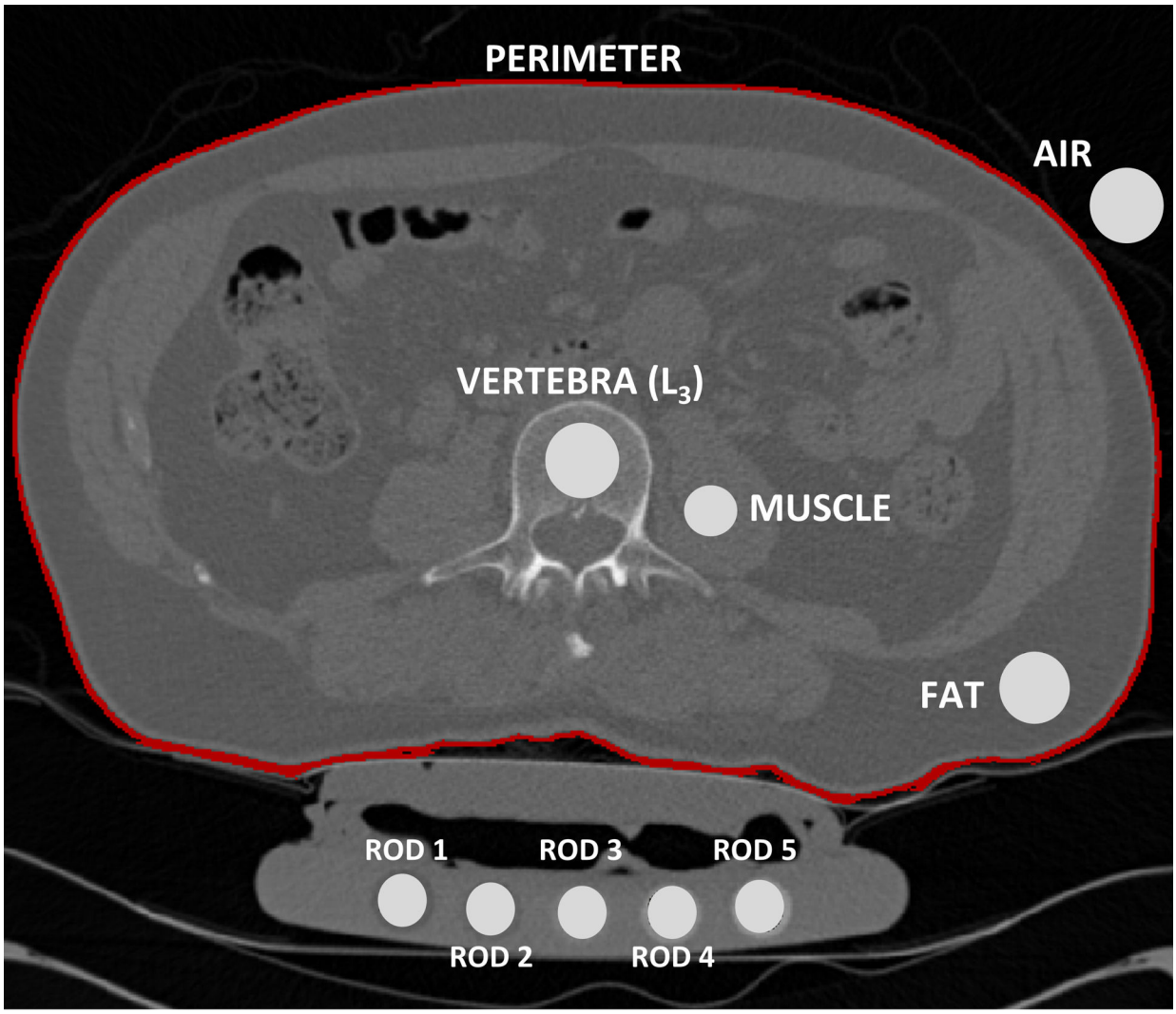

Figure 1.
Mean HU values were collected from the various ROIs on the L3 vertebra, psoas muscle, fat, air, and five phantom rods. Calibration phantom specifications were used to convert HU to BMD.

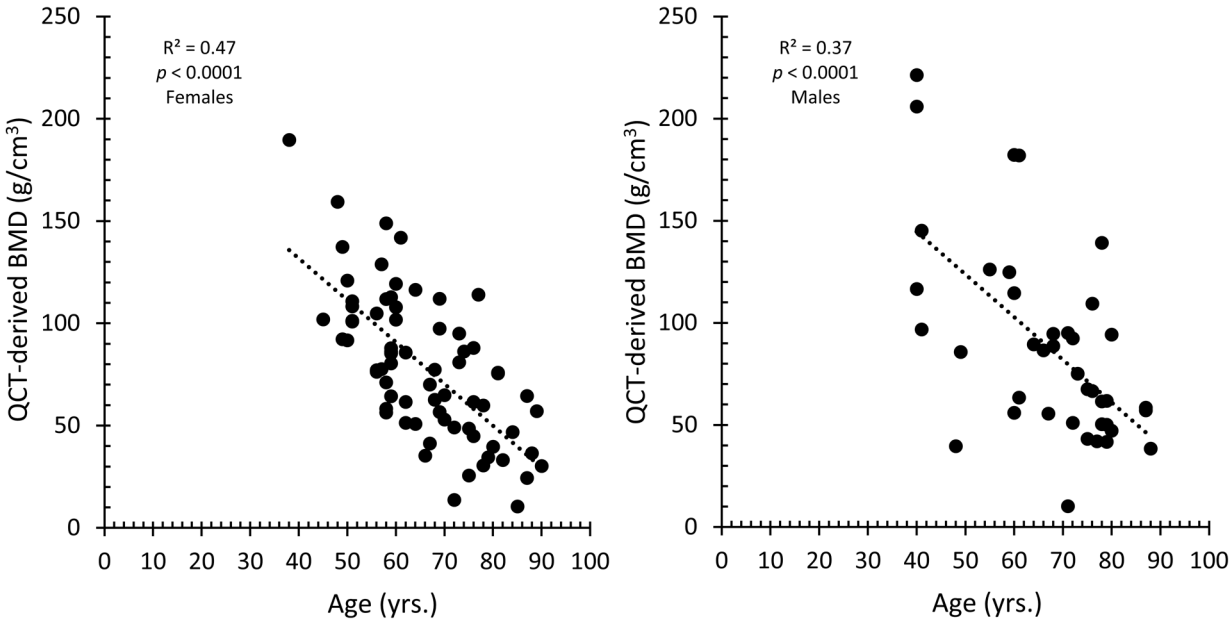

Figure 2.

Coefficient of determination (R^2) obtained for all 111 subjects to evaluate the effect of age on QCT-estimated BMD outcomes. BMD measurements were negatively correlated with age in both sexes (both $p<0.0001$).

Table 1.

Demographic information

		Cohort 1		
	Number of subjects	**Age (yrs.)**	**Height (cm)**	**Weight (kg)**
Men	30	67.2 ± 14.0	175.0 ± 7.5	89.7 ± 14.2
Female	50	64.3 ± 11.5	161.9 ± 5.3	73.4 ± 15.0
Total	80	65.4 ± 12.5	166.8 ± 8.9	79.5 ± 16.6
		Cohort 2		
	Number of subjects	**Age (yrs.)**	**Height (cm)**	**Weight (kg)**
Men	11	67.3 ± 14.0	177.1 ± 5.0	94.1 ± 15.1
Female	20	69.6 ± 13.1	161.3 ± 6.4	73.7 ± 16.0
Total	31	68.8 ± 13.2	166.9 ± 9.7	80.9 ± 18.3

Values are average ± standard deviation

Table 2.

Phantom-less equations coefficients and BMD correlations obtained using the phantom and phantom-less calibration methods.

Equations	Coefficients						$\widehat{R}^2$ (Y=X)
	C_1	C_2	C_3	C_4	C_5	C_6	
PAFM*	−10.75	−0.097	0.00005	0.003	−0.0020	0.8005	0.994
PFM	−10.99	−0.096	-	0.002	−0.0015	0.8005	0.994
AFM	−25.78	-	−0.00011	−0.057	−0.0181	0.8050	0.993
FM	−25.40	-	-	−0.055	−0.0193	0.8049	0.993
M	−20.28	-	-	-	−0.0020	0.8041	0.992

*P=Perimeter, A=Air, F=Fat, M=Muscle

Table 3.

Correlation outcomes between QCT/FEA fracture load estimates from the calibration phantom vs. phantom-less equations

	$\widehat{\mathbf{R}}^2$ **(accuracy; y=x)**
Average σ_{CT} and β_{CT}	0.99
PAFM	0.99
PFM	0.99
AFM	0.99
FM	0.98
M	0.94

Table 4.

QCT/FEA predicted fracture loads vs. aBMD from DXA

	Correlation outcomes (R^2)
Calibration Phantom	0.68
Average σ_{CT} and β_{CT}	0.68
PAFM	0.68
PFM	0.68
AFM	0.68
FM	0.64
M	0.67